SOME SOLUTIONS OF MINIMAXMAX PROBLEMS FOR THE TORSIONAL DISPLACEMENTS OF RECTANGULAR PLATES

PEDRO R.S. ANTUNES – FILIPPO GAZZOLA

Abstract. We consider an optimal shape problem aiming to reduce the torsional displacements of a partially hinged rectangular plate. The cost functional is the *gap function*, namely the maximum difference of displacements between the two free edges of the plate. We seek optimal shapes for reinforcements in order to minimize the gap function. This leads to a minimaxmax problem that we address both theoretically and numerically in some particular situations. Our results are in line with the expected behavior of bridges and they also give some hints for designs of future bridges.

Keywords: Shape optimization; partially hinged plates; torsional instability; bridges.
AMS Subject Classification (2010): 49Q10; 65K10; 35J40; 74K20.

1. Introduction

The deck of a suspension bridge may exhibit torsional oscillations which appear when the deck rotates around its main axis. These oscillations are extremely dangerous and may lead to collapses, see [9, §1.3,1.4] for a survey of some historical accidents. Following [8] we view the deck of a bridge as a long narrow rectangular thin plate Ω, hinged at two opposite edges and free on the remaining two edges: this plate well describes decks of suspension bridges which, at the short edges, are supported by the ground. Up to scaling, we may assume that the plate has length π and width 2ℓ with $2\ell \ll \pi$ so that

$$\Omega = (0,\pi) \times (-\ell,\ell) \subset \mathbb{R}^2 .$$

In [5, 8] the action of an external force f on this plate was modeled through the Kirchhoff-Love theory (see e.g. [23]): the energy $\mathbb{E}$ of the vertical displacement u of a plate Ω subject to a load f may be computed through the functional

$$\mathbb{E}(u) = EI \int_\Omega \left(\frac{(\Delta u)^2}{2} + (1-\sigma)(u_{xy}^2 - u_{xx}u_{yy}) \right) dxdy - \int_\Omega fu\, dxdy ,$$

where E is the Young modulus, I is the moment of inertia (so that EI is the flexural rigidity), σ is the Poisson ratio. Both the Young modulus and the Poisson ratio depend on the Lamé constants (see [23, (3.40)-(3.41)]) and, in particular,

$$0 < \sigma < \frac{1}{2} . \tag{1}$$

By (1) the energy functional $\mathbb{E}$ is convex. After dividing by EI and replacing f/EI with f, we may focus our attention on the scaled functional (still denoted by $\mathbb{E}$) defined by

$$\mathbb{E}(u) = \int_\Omega \left(\frac{(\Delta u)^2}{2} + (1-\sigma)(u_{xy}^2 - u_{xx}u_{yy}) - fu \right) dxdy . \tag{2}$$

The minimizer of $\mathbb{E}$ should then be multiplied by EI in order to recover the original meaning.

For the partially hinged plate under consideration, the functional $\mathbb{E}$ has to be minimized on the space

$$H^2_*(\Omega) := \Big\{ v \in H^2(\Omega) : \, v = 0 \text{ on } \{0,\pi\} \times (-\ell,\ell) \Big\} . \tag{3}$$

Since $\Omega \subset \mathbb{R}^2$, we have $H^2(\Omega) \subset C^0(\overline{\Omega})$ so that the condition on $\{0,\pi\} \times (-\ell,\ell)$ is satisfied pointwise.

Date: August 20, 2018.
P.A. was partially supported by FCT, Portugal, through the program "Investigador FCT" with reference IF/00177/2013 and the FCT scientific project PTDC/MAT- CAL/4334/2014. F.G. was partially supported by the PRIN project Equazioni alle derivate parziali di tipo ellittico e parabolico and by GNAMPA-INdAM.

The continuity of the minimizer u enables us to use the *gap function*

$$\mathcal{G}(x) := u(x,\ell) - u(x,-\ell) \qquad x \in (0,\pi) \tag{4}$$

introduced in [3]. The gap function measures the difference of the vertical displacements on the two free edges of the plate Ω and is therefore a measure of its torsional response, also in terms of its angle of torsion: by "free edge" we intend both $(0,\pi)\times\{\ell\}$ and $(0,\pi)\times\{-\ell\}$. The *maximal gap* is then computed by determining the maximum of the gap function:

$$\mathcal{G}^\infty := \max_{x\in[0,\pi]} \left|u(x,\ell) - u(x,-\ell)\right|. \tag{5}$$

This measures the torsional performance of the plate since the corresponding angle of rotation is

$$\theta = \arctan\frac{\mathcal{G}^\infty}{2\ell}. \tag{6}$$

Clearly, $\mathcal{G}^\infty$ and θ depend on f through the energy (2) and one is led to seek the function f (belonging to a suitable class $\mathcal{F}$) which yields the largest torsional displacement. Then, aiming to lower the torsional risk, one may strengthen the plate. Imagine that one has a certain amount of stiff material (mixture of steel and concrete) and has to decide where to place it within the deck of a bridge in order to lower the maximal gap $\mathcal{G}^\infty$ and, in turn, the torsional displacements. For economical reasons, this material should occupy only a proper open subset D of Ω, so that its measure satisfies $|D| \in (0, 2\ell\pi)$ and, possibly, further geometric constraints. The stiffening structure D reinforces only a part of the plate by a factor $(1+d)$, where $d>0$ is a constant measuring the additional strength of the stiffening material: this means that the stiff material is placed in some parts of the plate in order to increase the flexural rigidity and, therefore, the energy necessary to bend it. This kind of minimization problem naturally leads to homogenization [17], see also [14] for a stiffening problem for the torsion of a bar.

Our purpose is to minimize the maximal gap $\mathcal{G}^\infty$ which depends both on f and D: $\mathcal{G}^\infty = \mathcal{G}^\infty_{f,D}$. We introduce some classes $\mathcal{F}$ and $\mathcal{D}$ and we tackle the *minimaxmax problem*:

$$\min_{D\in\mathcal{D}} \max_{f\in\mathcal{F}} \max_{x\in[0,\pi]} \left|u(x,\ell) - u(x,-\ell)\right|, \tag{7}$$

where u is the minimizer of the energy functional. The existence of an optimal couple $(f,D)\in\mathcal{F}\times\mathcal{D}$ achieving the maximum and the minimum in (7) depend on how wide are the classes $\mathcal{F}$ and $\mathcal{D}$. Several different classes are considered in the present paper, see (24), (31), (32), (35), (42), (43) for $\mathcal{F}$ and (19), (34), (38), (40) for $\mathcal{D}$. We mostly restricted our attention to simple designs D that are appropriate for engineering applications.

The minimaxmax problem (7) can be also seen as a *worst-case optimization problem* [1, 7], since one is interested in minimizing the worst value of a functional among all possible designs. Some results about (7) were obtained in [4] but, since the problem is quite involved, several questions were left open. In this paper we give answers to some of these questions and we tackle further related problems with applications to suspension bridges. We restrict our attention to some particular problems of practical interest. We study the torsional stability of bridges as the Poisson ratio and the width vary and we give some suggestions for future designs of bridges. We also consider nonlinear problems aiming to model the stretching action of the sustaining cables and we analyze a model of cars going across the bridge.

This paper is organized as follows. In Section 2 we define in detail the minimaxmax problem, for both the linear and nonlinear models. In Section 3 we explain the procedure that we use for the numerical experiments. In Section 4 we focus on some problems left open in [4] for the free plate ($D=\emptyset$), in particular we numerically study in detail the worst case in L^p spaces and we formulate some new conjectures and open problems. In Sections 5 and 6 we address the minimaxmax problem (7) when the set $\mathcal{D}$ of admissible designs is formed by rectangles, as in suspension bridges: we study the dependence of the torsional response of the plate with respect to both its width 2ℓ and to the Poisson ratio σ. In Section 7 we consider the nonlinear minimaxmax problem in the case of a bridge crossed by a fixed number of cars.

2. Variational setting and energy of the reinforced plate

By [8, Lemma 4.1] we know that the space $H^2_*(\Omega)$ introduced in (3) is a Hilbert space when endowed with the scalar product

$$(u,v)_{H^2_*} := \int_\Omega \left[\Delta u \Delta v + (1-\sigma)(2u_{xy}v_{xy} - u_{xx}v_{yy} - u_{yy}v_{xx})\right] dxdy$$

and associated norm $\|u\|^2_{H^2_*} = (u,u)_{H^2_*}$, which is equivalent to the usual norm in $H^2(\Omega)$, that is, $\|u\|^2_{H^2} = \|u\|^2_{L^2} + \|D^2u\|^2_{L^2}$ where D^2u is the Hessian matrix of u. We also define

$$H^{-2}_*(\Omega) := \text{ the dual space of } H^2_*(\Omega)$$

and we denote by $\langle\cdot,\cdot\rangle$ the corresponding duality. If $f \in L^1(\Omega)$ then the functional $\mathbb{E}$ is well-defined in $H^2_*(\Omega)$, while if $f \in H^{-2}_*(\Omega)$ we need to replace $\int_\Omega fu$ with $\langle f, u\rangle$.

Assume that the plate Ω is reinforced with a stiff material which occupies an open region $D \subset \Omega$ and that D belongs to a certain class $\mathcal{D}$, while f belongs to some set $\mathcal{F}$ of admissible forcing terms. We stiffen the plate by increasing the cost of the bending energy, which modifies the original energy (2) into

$$\mathbb{E}_R(u) = \int_\Omega \left[(1+d\chi_D)\left(\frac{(\Delta u)^2}{2} + (1-\sigma)(u^2_{xy} - u_{xx}u_{yy})\right) - fu\right] dxdy\,, \tag{8}$$

where χ_D is the characteristic function of D and $d > 0$ is the additional strength of the stiffening material. Compared with the scaled energy (2), this amounts to *increasing the flexural rigidity EI by maintaining fixed the Poisson ratio* σ. As for (2), the functional $\mathbb{E}_R$ in (8) is convex and should be minimized on the space $H^2_*(\Omega)$. For all $f \in H^{-2}_*(\Omega)$ the unique minimizer of $\mathbb{E}_R$ satisfies the weak Euler-Lagrange equation

$$\int_\Omega (1+d\chi_D)\big[\Delta u\Delta v + (1-\sigma)(2u_{xy}v_{xy} - u_{xx}v_{yy} - u_{yy}v_{xx})\big]\, dxdy = \langle f, v\rangle \qquad \forall v \in H^2_*(\Omega)\,, \tag{9}$$

which has no strong counterpart due to the lack of regularity of the term $(1+d\chi_D)$ forbids to write the Euler-Lagrange equation in a strong form. Therefore, the minimizer $u_{f,D} \in H^2_*(\Omega)$ satisfies a weak Euler-Lagrange equation but not a strong one.

Assume that the two classes $\mathcal{F}$ and $\mathcal{D}$ of admissible f and D are fixed. Some examples of sets $\mathcal{F}$ and $\mathcal{D}$ will be given in Sections 4 and 5. Take $f \in \mathcal{F}$ and $D \in \mathcal{D}$ and the minimizer $u_{f,D} \in H^2_*(\Omega) \subset C^0(\overline{\Omega})$ of $\mathbb{E}_R$. Then compute its gap function and its maximal gap:

$$\mathcal{G}_{f,D}(x) = u_{f,D}(x,\ell) - u_{f,D}(x,-\ell)\,, \qquad \mathcal{G}^\infty_{f,D} = \max_{x\in[0,\pi]} |\mathcal{G}_{f,D}(x)|\,. \tag{10}$$

This defines the map

$$\mathcal{G}^\infty_{f,D} : \mathcal{F}\times\mathcal{D} \to [0,\infty)\,, \quad (f,D) \mapsto \mathcal{G}^\infty_{f,D}\,.$$

At this point, we first determine the worst $f \in \mathcal{F}$:

$$\mathcal{G}^\infty_D = \max_{f\in\mathcal{F}} \mathcal{G}^\infty_{f,D} = \max_{f\in\mathcal{F}} \max_{x\in[0,\pi]} |\mathcal{G}_{f,D}(x)|\,, \tag{11}$$

and then the best $D \in \mathcal{D}$:

$$\mathcal{G}^\infty = \min_{D\in\mathcal{D}} \mathcal{G}^\infty_D = \min_{D\in\mathcal{D}} \max_{f\in\mathcal{F}} \max_{x\in[0,\pi]} |\mathcal{G}_{f,D}(x)|\,. \tag{12}$$

This is the minimaxmax problem considered in the present paper. In the next sections we analyze some classes $\mathcal{F}$ and $\mathcal{D}$ where (12) admits a solution. Note that $\mathcal{G}^\infty = \mathcal{G}^\infty(\mathcal{F},\mathcal{D})$ is monotone with respect to both the classes $\mathcal{F}$ and $\mathcal{D}$ but with opposite monotonicity, see [4].

So far we merely considered linear problems, leading to a linear PDE, see (9). However, if one aims to use a plate model for a suspension bridge, then a linear theory is not sufficiently accurate. As pointed out in the engineering literature (see, e.g., [2, 16]), the most relevant source of nonlinearity in suspension bridges is due to the sustaining cables: in fact, "nonlinearity" is here synonymous of *contribution to torsion and instability*. Therefore, as in [16] we assume that the hangers connecting the

sustaining cables and the deck are inextensible. The effect of the cable action is concentrated on two small strips of Ω parallel to the free edges, that is,

$$\omega := (0,\pi) \times \left[\left(-\frac{\pi}{150}, -\frac{\pi}{150} + \frac{\pi}{1500} \right) \cup \left(\frac{\pi}{150} - \frac{\pi}{1500}, \frac{\pi}{150} \right) \right] . \tag{13}$$

This choice is motivated by the size of real bridges which have lengths of approximately 1km, width of approximately 13m, whereas the hangers are confined in strips of amplitude 1.3m close to the long edges of the plate, see a sketch in Figure 1.

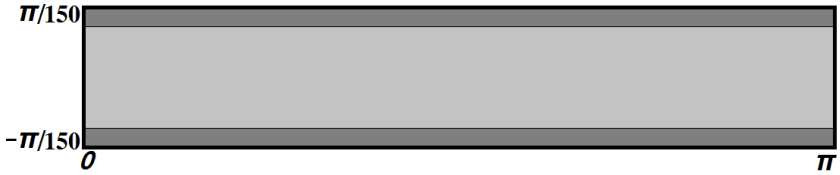

FIGURE 1. The plate Ω and its subset (dark grey) where the cables+hangers act.

This means that the deformation of each of the two strips in (13) is rigidly transmitted to the above sustaining cable whose *stretching* increases nonlinearly its tension and has a nonlocal effect distributed throughout the whole cable. In order to model this effect, we use the Woinowsky-Krieger [25] modification of the classical models by Bernoulli and Euler assuming a nonlinear dependence of the axial strain on the deformation gradient. Then the energy to be minimized is

$$\mathbb{N}(u) = \int_\Omega \left[(1 + d\chi_D) \left(\frac{(\Delta u)^2}{2} + (1-\sigma)(u_{xy}^2 - u_{xx}u_{yy}) \right) - fu \right] dxdy + \frac{1}{4} \left(\int_\omega u_x^2 \, dxdy \right)^2 , \tag{14}$$

which should be compared with (2). Note that only stretching in the x-direction is considered since the two (vertical) short edges are hinged. It is straightforward that the convex energy $\mathbb{N}$ admits a unique minimizer u for all $f \in H_*^{-2}(\Omega)$ and that u satisfies the weak Euler-Lagrange equation

$$\int_\Omega (1+d\chi_D) \big[\Delta u \Delta v + (1-\sigma)(2u_{xy}v_{xy} - u_{xx}v_{yy} - u_{yy}v_{xx}) \big] \, dxdy + \int_\omega u_x^2 \, dxdy \cdot \int_\omega u_x v_x \, dxdy = \langle f, v \rangle \tag{15}$$

for all $v \in H_*^2(\Omega)$ which, again, has no strong counterpart. After the solution of (15) is found, we follow the same procedure as for (10)-(11) and we reach again the minimaxmax problem (12).

For both the linear and nonlinear minimaxmax problems we obtain theoretical and numerical results, complemented with some conjectures and open problems. In the next section we illustrate the numerical procedure.

3. Numerical methods

In this section we give a brief description of the numerical algorithm for solving the minimaxmax problem (7). We consider the following sets of basis functions

$$\phi_{i,j}(x,y) = \sin(ix) \sin\left(\frac{j\pi(y-\ell)}{2\ell} \right), \quad \varphi_{i,j}(x,y) = \sin(ix) \cos\left(\frac{(j-1)\pi(y-\ell)}{2\ell} \right),$$

$$\psi_{i,j}(x,y) = \cos((i-1)x) \sin\left(\frac{j\pi(y-\ell)}{2\ell} \right), \quad \eta_{i,j}(x,y) = \cos((i-1)x) \cos\left(\frac{(j-1)\pi(y-\ell)}{2\ell} \right),$$

defined for $i,j = 1,2,...$ and the expansions

$$u(x,y) = \sum_{i=1}^{M} \sum_{j=1}^{N} a_{i,j}^u \phi_{i,j}(x,y) + \sum_{i=1}^{M} \sum_{j=1}^{N} b_{i,j}^u \varphi_{i,j}(x,y), \tag{16}$$

$$f(x,y) = \sum_{i=1}^{M} \sum_{j=1}^{N} a_{i,j}^f \phi_{i,j}(x,y) + \sum_{i=1}^{M} \sum_{j=1}^{N} b_{i,j}^f \varphi_{i,j}(x,y) + \sum_{i=1}^{M} \sum_{j=1}^{N} c_{i,j}^f \psi_{i,j}(x,y) + \sum_{i=1}^{M} \sum_{j=1}^{N} d_{i,j}^f \eta_{i,j}(x,y), \tag{17}$$

for some $M, N \in \mathbb{N}$. Note that, by construction, the approximation of u in (16) satisfies the homogenous boundary conditions on the small edges of the plate.

Remark 1. *Note that for some particular coefficients $a^u_{i,j}$ and $b^u_{i,j}$, the gap function is given by*

$$\begin{aligned}\mathcal{G}(x) &= u(x,\ell) - u(x,-\ell)\\ &= \sum_{i=1}^{M}\sum_{j=1}^{N} a^u_{i,j}\left(\phi_{i,j}(x,\ell) - \phi_{i,j}(x,-\ell)\right) + \sum_{i=1}^{M}\sum_{j=1}^{N} b^u_{i,j}\left(\varphi_{i,j}(x,\ell) - \varphi_{i,j}(x,-\ell)\right)\\ &= \sum_{i=1}^{M}\sum_{j=1}^{N} b^u_{i,j}\sin(ix)\left(1+(-1)^j\right)\end{aligned}$$

because $\phi_{i,j}(x,\ell) - \phi_{i,j}(x,-\ell) = 0$ and $\varphi_{i,j}(x,\ell) - \varphi_{i,j}(x,-\ell) = 1 + (-1)^j$.

Let us introduce the scalar product

$$(u,v)_D := \int_\Omega (1 + d\chi_D)\left[\Delta u \Delta v + (1-\sigma)(2u_{xy}v_{xy} - u_{xx}v_{yy} - u_{yy}v_{xx})\right] dxdy\,.$$

For a given function f, the numerical solution of (9) leads to a linear system of Galerkin equations,

$$\begin{cases} \sum_{i=1}^{M}\sum_{j=1}^{N}\left[a^u_{i,j}(\phi_{i,j},\phi_{k,m})_D + b^u_{i,j}(\varphi_{i,j},\phi_{k,m})_D\right] = \langle f, \phi_{k,m}\rangle \\ \sum_{i=1}^{M}\sum_{j=1}^{N}\left[a^u_{i,j}(\phi_{i,j},\varphi_{k,m})_D + b^u_{i,j}(\varphi_{i,j},\varphi_{k,m})_D\right] = \langle f, \varphi_{k,m}\rangle \end{cases}$$

for $k = 1, 2, ...M,\ m = 1, 2, ..., N$, which can be written as

$$\underbrace{\left[\begin{array}{c|c} (\phi_{i,j},\phi_{k,m})_D & (\varphi_{i,j},\phi_{k,m})_D \\ \hline (\phi_{i,j},\varphi_{k,m})_D & (\varphi_{i,j},\varphi_{k,m})_D \end{array}\right]}_{\mathbf{M}} \cdot \begin{bmatrix} a^u_{i,j} \\ b^u_{i,j} \end{bmatrix} = \begin{bmatrix} \langle f,\phi_{k,m}\rangle \\ \langle f,\varphi_{k,m}\rangle \end{bmatrix}. \tag{18}$$

In all the integrals involved in the previous linear system, the integrand is a product of trigonometric functions and can be calculated exactly, i.e., avoiding quadrature errors. For example we have,

$$\int_0^\pi \int_{-\ell}^{\ell} \phi_{i,j}(x,y)\phi_{k,m}(x,y)dydx = \begin{cases} \frac{\ell\pi}{2} & \text{if } i = k,\ j = m \\ 0 & \text{otherwise} \end{cases}$$

and all the remaining integrals can be calculated in a similar fashion.

Once we have solved the linear system (18), we obtain the coefficients $b^u_{i,j}$ and the gap function is calculated taking into account Remark 1 and we need to solve the optimization problem $\max_{x\in[0,\pi]} |\mathcal{G}_{f,D}(x)|$, for example using a direct search method. We will denote by X a point in $[0,\pi]$, for which

$$\max_{x\in[0,\pi]} |\mathcal{G}_{f,D}(x)| = |\mathcal{G}(X)|.$$

Again, taking into account Remark 1, we observe that

$$\frac{\partial\left(\mathcal{G}(X)\right)}{\partial\left(a^u_{i,j}\right)} = 0, \quad \frac{\partial\left(\mathcal{G}(X)\right)}{\partial\left(b^u_{i,j}\right)} = \sin(iX)(1+(-1)^j).$$

Next step is the calculation of $\mathcal{G}^\infty_D$, that is, we seek the optimal $f \in \mathcal{F}$ that allows to obtain the maximal gap function: we consider different classes $\mathcal{F}$ specified in the applications, see (24), (31), (32), (35), (42), (43). We assume that f is given by (17) and we determine optimal coefficients $a^f_{i,j}$, $b^f_{i,j}$, $c^f_{i,j}$ and $d^f_{i,j}$ by a gradient type method. In particular, it is convenient to know how does the gap function changes, once we perturb each of those coefficients. Taking into account (18), we have that

the derivative of the coefficients $a^u_{i,j}$, $b^u_{i,j}$ with respect to a perturbation of each coefficient defining f can be obtained through the solution of a linear system,

$$\mathbf{M}.\begin{bmatrix} \frac{\partial(a^u_{i,j})}{\partial a^f_{i,j}} \\ \frac{\partial(b^u_{i,j})}{\partial a^f_{i,j}} \end{bmatrix} = \begin{bmatrix} \langle \phi_{i,j}, \phi_{k,m} \rangle \\ \langle \phi_{i,j}, \varphi_{k,m} \rangle \end{bmatrix}, \quad \mathbf{M}.\begin{bmatrix} \frac{\partial(a^u_{i,j})}{\partial b^f_{i,j}} \\ \frac{\partial(b^u_{i,j})}{\partial b^f_{i,j}} \end{bmatrix} = \begin{bmatrix} \langle \varphi_{i,j}, \phi_{k,m} \rangle \\ \langle \varphi_{i,j}, \varphi_{k,m} \rangle \end{bmatrix}$$

$$\mathbf{M}.\begin{bmatrix} \frac{\partial(a^u_{i,j})}{\partial c^f_{i,j}} \\ \frac{\partial(b^u_{i,j})}{\partial c^f_{i,j}} \end{bmatrix} = \begin{bmatrix} \langle \psi_{i,j}, \phi_{k,m} \rangle \\ \langle \psi_{i,j}, \varphi_{k,m} \rangle \end{bmatrix}, \quad \mathbf{M}.\begin{bmatrix} \frac{\partial(a^u_{i,j})}{\partial d^f_{i,j}} \\ \frac{\partial(b^u_{i,j})}{\partial d^f_{i,j}} \end{bmatrix} = \begin{bmatrix} \langle \eta_{i,j}, \phi_{k,m} \rangle \\ \langle \eta_{i,j}, \varphi_{k,m} \rangle \end{bmatrix}.$$

Finally, we have

$$\frac{\partial(\mathcal{G}(X))}{\partial\left(a^f_{i,j}\right)} = \frac{\partial(\mathcal{G}(X))}{\partial\left(b^u_{i,j}\right)}\frac{\partial\left(b^u_{i,j}\right)}{\partial\left(a^f_{i,j}\right)}, \quad \frac{\partial(\mathcal{G}(X))}{\partial\left(b^f_{i,j}\right)} = \frac{\partial(\mathcal{G}(X))}{\partial\left(b^u_{i,j}\right)}\frac{\partial\left(b^u_{i,j}\right)}{\partial\left(b^f_{i,j}\right)}$$

$$\frac{\partial(\mathcal{G}(X))}{\partial\left(c^f_{i,j}\right)} = \frac{\partial(\mathcal{G}(X))}{\partial\left(b^u_{i,j}\right)}\frac{\partial\left(b^u_{i,j}\right)}{\partial\left(c^f_{i,j}\right)}, \quad \frac{\partial(\mathcal{G}(X))}{\partial\left(d^f_{i,j}\right)} = \frac{\partial(\mathcal{G}(X))}{\partial\left(b^u_{i,j}\right)}\frac{\partial\left(b^u_{i,j}\right)}{\partial\left(d^f_{i,j}\right)}.$$

The last step of the numerical procedure is to solve the optimization problem (12). For this purpose, we consider $\mathcal{D}$ to be the union of P disjoint rectangles of a fixed size (as for real bridges, see Section 5),

$$\mathcal{D} = \bigcup_{j=1}^{P} \left(\left[x_j - \frac{\Delta x}{2}, x_j + \frac{\Delta x}{2} \right] \times \left[y_j - \frac{\Delta y}{2}, y_j + \frac{\Delta y}{2} \right] \right), \tag{19}$$

for $x_j \in \left[\frac{\Delta x}{2}, \pi - \frac{\Delta x}{2}\right]$ and $y_j \in \left[-\ell + \frac{\Delta y}{2}, \ell - \frac{\Delta y}{2}\right]$. Then, we define a vector $\mathcal{V} = (x_1, ..., x_P, y_1, ..., y_P)$ and the optimization (12) is solved by searching for optimal vectors $\mathcal{V}$. This optimization was performed by a pattern search numerical method using Matlab Routine `patternsearch`. This is a numerical method to minimize functions without the use of derivatives or approximations of derivatives of the objective function (see for example [22]). In next sections we will present some numerical results obtained with the previous algorithm for solving the minimaxmax problem. In most cases, in the numerical simulations we took the discretization parameters $M = 35$, $N = 20$.

4. Worst case for the free plate

In the case of a free plate ($D = \emptyset$) the energy $\mathbb{E}_R$ in (8) coincides with $\mathbb{E}$ in (2). Up to a multiplicative constant, the Euler-Lagrange equation satisfied by the minimizer of the energy (2) reads

$$\Delta^2 u = f \qquad \text{in } \Omega\,, \tag{20}$$

complemented with the boundary conditions

$$u(0,y) = u_{xx}(0,y) = u(\pi,y) = u_{xx}(\pi,y) = 0 \qquad \forall y \in (-\ell,\ell) \tag{21}$$

on the short edges where the plate is hinged and

$$u_{yy}(x,\pm\ell) + \sigma u_{xx}(x,\pm\ell) = 0\,, \quad u_{yyy}(x,\pm\ell) + (2-\sigma)u_{xxy}(x,\pm\ell) = 0 \quad \forall x \in (0,\pi) \tag{22}$$

on the large edges where the plate is free. We refer to [24, (2.40)] for the justification of these boundary conditions, see also [8] for full details on how to derive them for the rectangular plate Ω under study. The behavior of rectangular plates subject to a variety of boundary conditions is studied in [6, 10, 11, 18]. The solution u of (20)-(21)-(22) represents the vertical displacement of the plate under the action of f and, since the boundary conditions (21)-(22) satisfy the complementing condition [8, Lemma 4.2] so that elliptic regularity applies, u is a strong solution of (20) whenever f belongs to suitable spaces.

One is then interested in solving the maxmax problem

$$\max_{f\in\mathcal{F}} \mathcal{G}_f^\infty = \max_{f\in\mathcal{F}} \max_{x\in[0,\pi]} \big|u(x,\ell) - u(x,-\ell)\big|\,, \tag{23}$$

where $u \in H^2_*(\Omega)$ is the minimizer of $\mathbb{E}$ and depends on f through (20).

In this section we seek the optimal (worst) force f within the class

$$\mathcal{F} = \{f \in L^p(\Omega);\, \|f\|_p = 1\}\,, \qquad 1 \leqslant p \leqslant \infty\,. \tag{24}$$

This problem was left open in [4], although partial results were obtained and several conjectures were made. From [4, Section 4] we recall that the worst f exists and is necessarily odd with respect to y whenever $1 < p < \infty$; for $p = \infty$ existence is known and symmetry is expected (but not fully proved), while nonexistence of a worst f is expected when $p = 1$.

4.1. **Large values of p.** In Figure 2 we represent the numerically obtained level sets of the worst normalized f when $p = 10$, $p = 50$ and $p = \infty$.

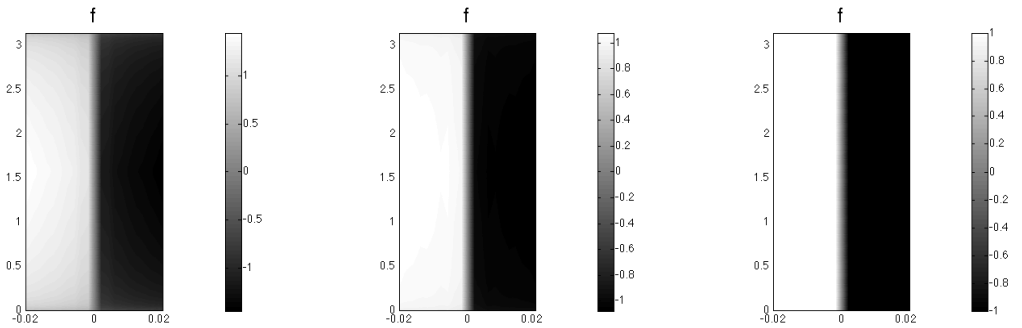

FIGURE 2. Worst normalized $f \in L^p(\Omega)$ when $D = \emptyset$, for $p = 10$ (left plot), $p = 50$ (middle plot) and $p = \infty$ (right plot). The x-axis is vertical, the y-axis is horizontal.

Overall, Figure 2 suggests the following conjecture.

Conjecture 2. *If $\mathcal{F} = \{f \in L^\infty(\Omega);\, \|f\|_\infty = 1\}$, then the solution f of the maxmax problem* (23) *is given by both the odd functions $\pm f$, where*

$$f(x,y) = \begin{cases} 1 & \text{if } y > 0 \\ -1 & \text{if } y < 0\,. \end{cases} \tag{25}$$

If Conjecture 2 were true, then one would be able to find the value in (23).

Proposition 3. *Let f be as in* (25)*. Then, for all $x \in (0,\pi)$, we have the explicit form of the gap function* (4)

$$\mathcal{G}(x) = \frac{8}{(1-\sigma)\pi} \sum_{k=0}^{\infty} \frac{\Big(\cosh\big[(2k+1)\ell\big] - 1\Big)\Big((3-\sigma)\sinh\big[(2k+1)\ell\big] - (1-\sigma)(2k+1)\ell\Big)}{\Big[(3+\sigma)\sinh\big[(2k+1)\ell\big]\cosh\big[(2k+1)\ell\big] + (1-\sigma)(2k+1)\ell\Big](2k+1)^5} \sin[(2k+1)x]\,.$$

Proof. For f as in (25), we seek the strong solution u of the problem

$$\begin{cases} \Delta^2 u = f & \text{in } \Omega \\ u(0,y) = u_{xx}(0,y) = u(\pi,y) = u_{xx}(\pi,y) = 0 & \text{for } y \in (-\ell,\ell) \\ u_{yy}(x,\pm\ell) + \sigma u_{xx}(x,\pm\ell) = u_{yyy}(x,\pm\ell) + (2-\sigma)u_{xxy}(x,\pm\ell) = 0 & \text{for } x \in (0,\pi)\,. \end{cases}$$

By uniqueness of the solution, u is odd with respect to y and it suffices to solve the Euler-Lagrange equation associated to the energy (2), that is,

$$
\begin{cases}
\Delta^2 u = 1 & \text{in } (0,\pi)\times(0,\ell) \\
u(0,y) = u_{xx}(0,y) = u(\pi,y) = u_{xx}(\pi,y) = 0 & \text{for } y\in(0,\ell) \\
u(x,0) = u_{yy}(x,0) = 0 & \text{for } x\in(0,\pi) \\
u_{yy}(x,\ell) + \sigma u_{xx}(x,\ell) = u_{yyy}(x,\ell) + (2-\sigma)u_{xxy}(x,\ell) = 0 & \text{for } x\in(0,\pi)\,.
\end{cases} \tag{26}
$$

By separating variables, we seek the solution of (26) in the form

$$
u(x,y) = \sum_{n=1}^{\infty} \alpha_n(y)\sin(nx)\,.
$$

By recalling that

$$
1 = \frac{4}{\pi}\sum_{k=0}^{\infty}\frac{\sin[(2k+1)x]}{2k+1} \qquad \text{in } L^2(0,\pi)\,,
$$

this leads to

$$
\sum_{n=1}^{\infty}\left[\alpha_n''''(y) - 2n^2\alpha_n''(y) + n^4\alpha_n(y)\right]\sin(nx) = \frac{4}{\pi}\sum_{k=0}^{\infty}\frac{\sin[(2k+1)x]}{2k+1}
$$

which immediately shows that $\alpha_{2k}(y)\equiv 0$ and that the odd Fourier coefficients α_{2k+1} solve the equation

$$
\alpha_{2k+1}''''(y) - 2(2k+1)^2\alpha_{2k+1}''(y) + (2k+1)^4\alpha_{2k+1}(y) = \frac{4}{(2k+1)\pi}\,. \tag{27}
$$

Moreover, from the boundary conditions in (26) in $y=0$ and $y=\ell$, we infer that α_{2k+1} satisfies

$$
\alpha_{2k+1}(0) = \alpha_{2k+1}''(0) = \alpha_{2k+1}''(\ell) - \sigma(2k+1)^2\alpha_{2k+1}(\ell) = \alpha_{2k+1}'''(\ell) - (2-\sigma)(2k+1)^2\alpha_{2k+1}'(\ell) = 0\,. \tag{28}
$$

The solution of (27)-(28) is given by

$$
\begin{aligned}
\alpha_{2k+1}(y) \;=\; & \tfrac{4(3+\sigma)(1-\sigma)\cosh^2[(2k+1)\ell]+4\sigma(1+\sigma)\cosh[(2k+1)\ell]-4\sigma(1-\sigma)(2k+1)\ell\sinh[(2k+1)\ell]-2(1-\sigma)^2(2k+1)^2\ell^2-4(3-\sigma)}{(1-\sigma)\pi[(3+\sigma)\sinh[(2k+1)\ell]\cosh[(2k+1)\ell]+(1-\sigma)(2k+1)\ell](2k+1)^5}\sinh[(2k+1)y] \\
& + \tfrac{2(3-\sigma)+4\sigma\cosh[(2k+1)\ell]-2(3+\sigma)\cosh^2[(2k+1)\ell]}{\pi[(3+\sigma)\sinh[(2k+1)\ell]\cosh[(2k+1)\ell]+(1-\sigma)(2k+1)\ell](2k+1)^4}y\cosh[(2k+1)y] \\
& + \tfrac{2}{(2k+1)^4\pi}y\sinh[(2k+1)y] - \tfrac{4}{(2k+1)^5\pi}\cosh[(2k+1)y] + \tfrac{4}{(2k+1)^5\pi}
\end{aligned}
$$

so that

$$
\alpha_{2k+1}(\ell) = \frac{4}{(1-\sigma)\pi}\frac{\Big(\cosh\big[(2k+1)\ell\big]-1\Big)\Big((3-\sigma)\sinh\big[(2k+1)\ell\big]-(1-\sigma)(2k+1)\ell\Big)}{\Big[(3+\sigma)\sinh\big[(2k+1)\ell\big]\cosh\big[(2k+1)\ell\big]+(1-\sigma)(2k+1)\ell\Big](2k+1)^5}
$$

and then

$$
u(x,\ell) = \frac{4}{(1-\sigma)\pi}\sum_{k=0}^{\infty}\frac{\Big(\cosh\big[(2k+1)\ell\big]-1\Big)\Big((3-\sigma)\sinh\big[(2k+1)\ell\big]-(1-\sigma)(2k+1)\ell\Big)}{\Big[(3+\sigma)\sinh\big[(2k+1)\ell\big]\cosh\big[(2k+1)\ell\big]+(1-\sigma)(2k+1)\ell\Big](2k+1)^5}\sin[(2k+1)x]
$$

for all $x\in(0,\pi)$. In turn, since $y\mapsto u(x,y)$ is odd, we obtain the stated form for $\mathcal{G}_f(x)$. □

In order to compute the maximal gap $\mathcal{G}_f^\infty$ we make a couple of remarks and then proceed numerically. For f as in (25), it is straightforward that

$$
\mathcal{G}_f\left(\frac{\pi}{2}-x\right) = \mathcal{G}_f\left(\frac{\pi}{2}+x\right) \quad \forall x\in\left(0,\frac{\pi}{2}\right)\,, \qquad \mathcal{G}_f'\left(\frac{\pi}{2}\right) = 0\,;
$$

all this plays in favor of the natural conjecture that $\mathcal{G}_f^\infty = \mathcal{G}_f(\pi/2)$, which appears difficult to prove in full detail. There is also numerical evidence in favor of this conjecture: by plotting numerically the

graph of $x \mapsto \mathcal{G}_f(x)$, one sees that it is strictly concave with a unique maximum at $x = \pi/2$. Assuming this conjecture to be true, from Proposition 3 we would infer that

$$\mathcal{G}_f^\infty = \frac{8}{(1-\sigma)\pi} \sum_{k=0}^{\infty} (-1)^k \frac{\Big(\cosh\big[(2k+1)\ell\big] - 1\Big)\Big((3-\sigma)\sinh\big[(2k+1)\ell\big] - (1-\sigma)(2k+1)\ell\Big)}{\Big[(3+\sigma)\sinh\big[(2k+1)\ell\big]\cosh\big[(2k+1)\ell\big] + (1-\sigma)(2k+1)\ell\Big](2k+1)^5}\,.$$

Clearly, $\mathcal{G}_f^\infty$ depends on ℓ and σ. In Figure 3 we plot the map $\sigma \mapsto \mathcal{G}_f^\infty$ when the Poisson ratio σ varies in the "physical range" (1) and the map $\ell \mapsto \mathcal{G}_f^\infty/\ell$ when ℓ varies the shape of the plate from a beam to a square. Both plots are obtained by maintaining fixed the other variable.

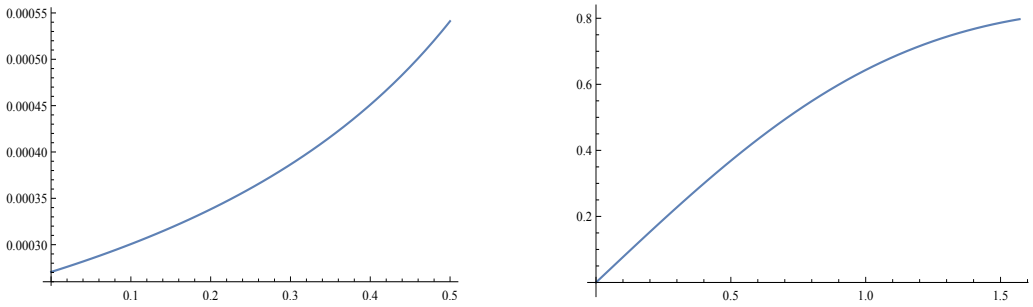

FIGURE 3. The map $\sigma \mapsto \mathcal{G}_f^\infty$ for f as in (25), $\ell = \frac{\pi}{150}$ and $\sigma \in [0, 1/2]$ (left) and the map $\ell \mapsto \mathcal{G}_f^\infty/\ell$ for f as in (25), $\sigma = 0.2$ and $\ell \in (0, \frac{\pi}{2}]$ (right).

The Poisson ratio is the negative ratio of transverse to axial strain: when a material is compressed in one direction, it tends to expand in the other two directions, see [23]. The Poisson ratio σ is a measure of this effect, it is the fraction of expansion divided by the fraction of compression for small values of these changes. For metals the value of σ lies around 0.3 while for concrete $0.1 < \sigma < 0.2$: the deck of a bridge is a mixture of iron and concrete. The left plot in Figure 3 shows that $\sigma \mapsto \mathcal{G}_f^\infty$ is increasing, which means that

(29) **in order to lower the torsional effects,**
one should put more concrete than metal in the deck of a bridge.

The right plot in Figure 3 shows that not only $\ell \mapsto \mathcal{G}_f^\infty$ is increasing (which had to be expected) but also that

(30) **the maximal gap increases superlinearly with respect to the width of the plate**

and this result well describes the fact that if $\ell \to 0$ then Ω behaves like a beam while if ℓ is comparable to π then Ω behaves like a plate. Indeed, the map $\ell \mapsto \mathcal{G}_f^\infty$ has initially a quadratic behavior and then it tends to behave linearly.

4.2. **Small values of p.** In Figure 4 we represent the numerically obtained level sets of the worst normalized f when $p = 1.1$, $p = 2$, and $p = 3$.

The maximization procedure did not converge to an optimal f when $p = 1$ and therefore we expect further that there is no worst case among normalized $f \in L^1(\Omega)$. The maximizing sequence exhibited spikes with opposite signs in the boundary points $(\frac{\pi}{2}, \pm\frac{\pi}{150})$ suggesting a weak*-convergence to deltas concentrated in these points.

In fact, from a physical point of view, it is more natural to consider the class

$$\mathcal{F} = \{f \in L^\infty(\Omega);\ \|f\|_1 = 1,\ \|f\|_\infty \leqslant M\} \tag{31}$$

for some $M > 0$. The constraint $\|f\|_1 = 1$ measures the total mass present on the plate whereas M measures the maximum mass density on the plate. The following statement is straightforward.

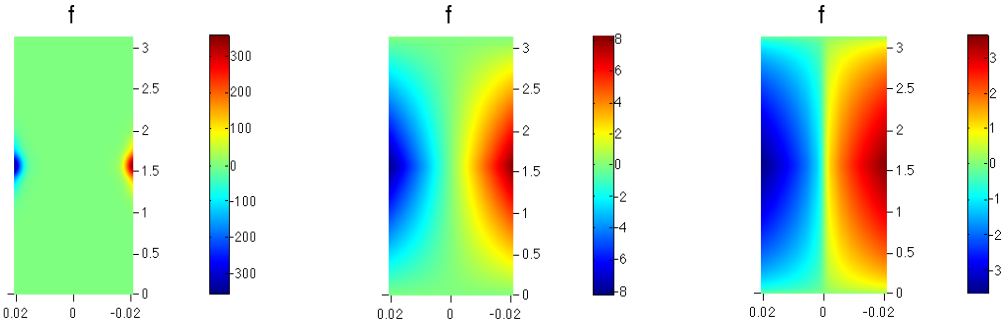

FIGURE 4. Worst normalized $f \in L^p(\Omega)$ when $D = \emptyset$, when $p = 1.1$ (left), $p = 2$ (middle), and $p = 3$ (right). The x-axis is vertical, the y-axis is horizontal.

Proposition 4. *Let $\mathcal{F}$ be as in* (31) *for some $M > 0$. Then the maxmax problem (23) admits a solution $f \in \mathcal{F}$.*

Proof. The class $\mathcal{F}$ is a bounded equi-integrable subset of $L^1(\Omega)$. Therefore, a maximizing sequence $\{f_n\} \subset \mathcal{F}$ converges weakly in $L^1(\Omega)$ to some $f \in L^1(\Omega)$, up to a subsequence. By L^∞-boundedness, it also converges weakly* in $L^\infty(\Omega)$. By lower semicontinuity of the L^1-norm with respect to weak convergence we have $\|f\|_1 \leqslant 1$ and by lower semicontinuity of the L^∞-norm with respect to weak* convergence we have $\|f\|_\infty \leqslant M$.

The weak convergence $f_n \rightharpoonup f$ in the L^p spaces implies the uniform convergence of the solutions of (20) and, in turn, of the gap functions. □

In Figure 5 we show two profiles of the solution of the maxmax problem (23), for $\mathcal{F}$ as in (31) with $M = 100$.

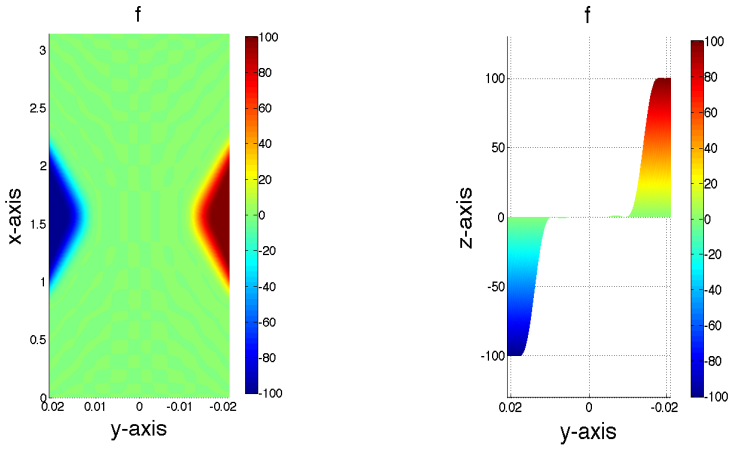

FIGURE 5. Two profiles of the solution of the maxmax problem (23), for $\mathcal{F}$ as in (31) with $M = 100$.

Therefore, with a physical constraint such as given maximum mass density, also the maximization problem in $L^1(\Omega)$ admits a solution. Without this constraint, we now give further numerical arguments in favor of the conjecture that maximizing sequences in $L^1(\Omega)$ weakly*-converge to the deltas concentrated in the boundary points $(\frac{\pi}{2}, \pm\frac{\pi}{150})$. For any $(z, w) \in \overline{\Omega}$ we consider the *odd* distribution

$$T_{z,w} := \frac{\delta_{(z,w)} - \delta_{(z,-w)}}{2},$$

where δ_P is the Dirac delta with mass concentrated at $P \in \overline{\Omega}$. Then we introduce the class of all such distributions:

$$\mathcal{F} = \{T_{z,w};\ (z,w) \in \overline{\Omega}\}\,. \tag{32}$$

We numerically computed the gap function for all $T \in \mathcal{F}$ with $\mathcal{F}$ as in (32) and the results showed that the maxmax problem (23) has the following solution:

$$\max_{T\in\mathcal{F}} \mathcal{G}_T^\infty = \mathcal{G}_{T_{\frac{\pi}{2},\ell}}^\infty \approx 0.1423.$$

In Figure 6 we represent the level lines of the map $(z,w) \mapsto \mathcal{G}_{T_{z,w}}^\infty$ when $(z,w) \in [0,\frac{\pi}{2}] \times [0,\frac{\pi}{150}]$; these lines, usually called *influence lines* [15], should then be extended by symmetry in the remaining parts of $\overline{\Omega}$. This figure was generated by evaluating the map at nodes of a grid built with 50 and 20 divisions, respectively, in the z and w directions.

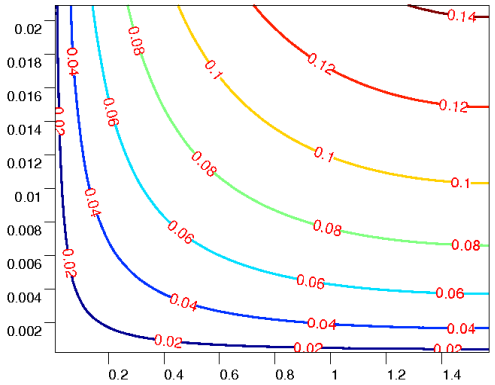

FIGURE 6. Level lines of $\mathcal{G}_T^\infty$ for $T \in \mathcal{F}$ defined by (32), with $(z,w) \in [0,\frac{\pi}{2}] \times [0,\frac{\pi}{150}]$.

Therefore, we are led to another conjecture.

Conjecture 5. *Let $\mathcal{F}$ be as in* (32)*. Then the solution f of the maxmax problem* (23) *is given by both the odd distributions $T_{\frac{\pi}{2},\pm\ell}$.*

If Conjecture 5 was true, then from [4, Section 4] one finds the value in (23):

$$\max_{(z,w)\in\overline{\Omega}} \mathcal{G}_{T_{z,w}}^\infty = \mathcal{G}_{T_{\frac{\pi}{2},\ell}}^\infty = \frac{2\sqrt{2}}{\sqrt{\pi(1-\sigma)}} \left[\sum_{k=0}^{\infty} \frac{\sinh^2[(2k+1)\ell]}{(2k+1)^3\left[(3+\sigma)\sinh[(2k+1)\ell]\cosh[(2k+1)\ell]+(1-\sigma)(2k+1)\ell\right]}\right]^{1/2}.$$

In Figure 7, we plot the maps $\sigma \mapsto \mathcal{G}_{T_{\frac{\pi}{2},\ell}}^\infty$ and $\ell \mapsto \mathcal{G}_{T_{\frac{\pi}{2},\ell}}^\infty$.

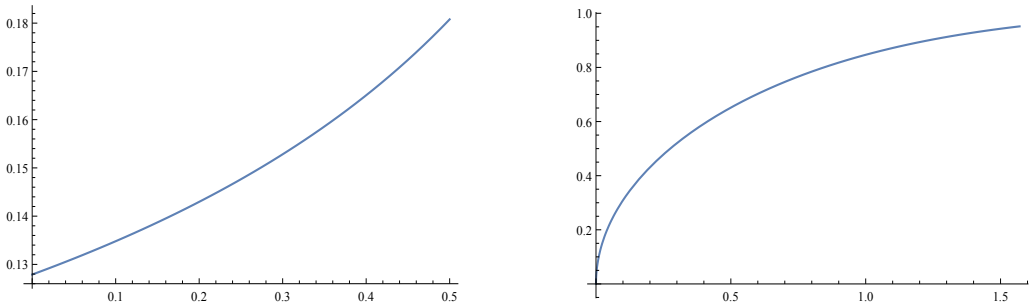

FIGURE 7. The map $\sigma \mapsto \mathcal{G}_{T_{\frac{\pi}{2},\ell}}^\infty$, when $\ell = \frac{\pi}{150}$ and $\sigma \in [0,1/2]$ (left) and the map $\ell \mapsto \mathcal{G}_{T_{\frac{\pi}{2},\ell}}^\infty$, when $\sigma = 0.2$ and $\ell \in (0,\frac{\pi}{2}]$ (right).

Also the left plot in Figure 7 shows that the maximal gap is an increasing function of σ, which confirms principle (29): we obtained the same picture for other values of ℓ. The right picture in Figure 7 shows that the growth with respect to ℓ is *sublinear*; from (6) we then deduce that the angle of rotation of the plate tends to $\pi/2$ as $\ell \to 0$ and to 0 as $\ell \to \infty$, as had to be expected: we obtained the same picture for other values of σ. This confirms that $\mathcal{G}^\infty$ is a reliable measure of the torsional performances of a partially hinged rectangular plate.

Finally, we illustrate the results that are obtained for different choices of M and N. We denote by $\mathcal{G}^{\infty,M,N}_{T_{\frac{\pi}{2},\ell}}$ the numerical approximation for $\mathcal{G}^\infty_{T_{\frac{\pi}{2},\ell}}$, obtained with the algorithm described in Section 3, taking a particular choice of M and N. In Figure 8 we plot the relative error,

$$E_{M,N} := \frac{\left|\mathcal{G}^{\infty,M,N}_{T_{\frac{\pi}{2},\ell}} - \mathcal{G}^\infty_{T_{\frac{\pi}{2},\ell}}\right|}{\mathcal{G}^\infty_{T_{\frac{\pi}{2},\ell}}},$$

for $M = 10, 11, ..., 300$ and $N = 10, 11, ..., 20$. We observe that the algorithm is highly accurate. For example, taking $M = 300$ and $N = 20$ we obtain an error of 0.00675%.

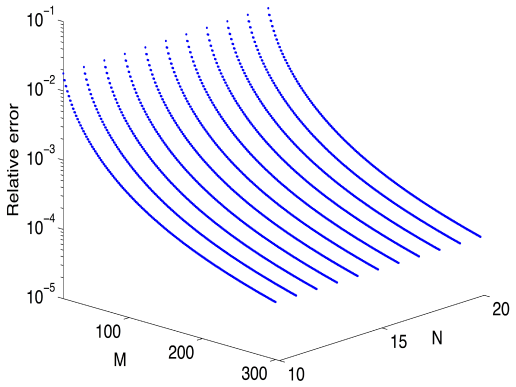

FIGURE 8. Convergence results for $E_{M,N}$, for $M = 10, 11, ..., 300$ and $N = 10, 11, ..., 20$.

5. Optimal reinforcements made of large rectangles

In order to justify reinforcements made of large rectangles, let us recall the main components of a suspension bridge and the technique of erection. We are here concerned with the main span, namely the part of the deck between the four towers. It has a rectangular shape with two long free edges (of the order of 1km) and two shorter edges (of the order of 15m) fixed and hinged between the towers. This is modeled by our plate Ω, where a reasonable choice of ℓ is $\ell = \pi/150$.

A suspension bridge is usually erected starting from the anchorages and the towers. Then the sustaining cables are installed between the two couples of towers and the hangers are hooked to the cables. Once all these components are in position, they furnish a stable working base from which the deck can be raised from floating barges, see Figure 9.

We refer to [20, Section 15.23] for full details. The deck segments are put in position one aside the other and have the shape of (large) rectangles. Our purpose is here to decide which of these segments (rectangles) should be made of a more stiff material. We will consider the optimizations of the rectangles to be stiffened, for two cases of forces f.

5.1. Optimal reinforcements with forces with unitary L^2 norm.

We divide the deck Ω into 20 rectangles (the deck segments), see Figure 10.

If $\Omega = (0, \pi) \times (-\frac{\pi}{150}, \frac{\pi}{150})$, then the k-th deck segment ($k = 1, ..., 20$) is the rectangle

$$R_k = \left(\frac{(k-1)\pi}{20}, \frac{k\,\pi}{20}\right) \times \left(-\frac{\pi}{150}, \frac{\pi}{150}\right). \tag{33}$$

FIGURE 9. Placement of the deck segments during the construction of suspension bridge.

FIGURE 10. Deck segments in the plate: 20 identical rectangles partitioning Ω.

We seek the optimal position of 4 stiffened segments R_k among the 20 so that

$$\mathcal{D} = \text{ the set of reunions of 4 rectangles } R_k \text{ as in (33)} \tag{34}$$

and $|D| = \pi^2/225$ for all $D \in \mathcal{D}$. Then we take

$$\mathcal{F} = \{f \in L^2(\Omega);\ \|f\|_2 = 1\} \tag{35}$$

and we compute numerically the gap function for all the possible 4,845 configurations (the binomial of 20 and 4). Due to possible symmetries, some of them are equivalent. We found that the optimal shape is $R_1 \cup R_3 \cup R_{18} \cup R_{20}$, see the picture in Figure 11 where gray rectangles are the stiffened segments of deck.

FIGURE 11. Solution of the minimaxmax problem (7) for $\mathcal{D}$ and $\mathcal{F}$ as in (34)-(35).

For any $D \in \mathcal{D}$, we computed the value defined in (11) and the corresponding angle of rotation defined in (6). The extremal values were obtained for

$$D = R_1 \cup R_3 \cup R_{18} \cup R_{20} \implies \mathcal{G}_D^\infty \approx 1.054 \cdot 10^{-3}\ (\theta \approx 2.515 \cdot 10^{-2})$$

$$D = R_9 \cup R_{10} \cup R_{11} \cup R_{12} \implies \mathcal{G}_D^\infty \approx 1.154 \cdot 10^{-3}\ (\theta \approx 2.882 \cdot 10^{-2})\,.$$

In between were the values of all the other configurations $D \in \mathcal{D}$, with $\mathcal{D}$ as in (34): in particular, we mention that the second best set of segments was

$$D = R_2 \cup R_4 \cup R_{18} \cup R_{20} \implies \mathcal{G}_D^\infty \approx 1.056 \cdot 10^{-3}\ (\theta \approx 2.519 \cdot 10^{-2}).$$

The results clearly emphasized that

(36) **in order to lower the torsional effects, it is better to place (symmetric) reinforcements close to the hinged edges rather than close to midspan.**

With this criterion at hand, we refined the experiment by taking smaller deck segments, with half length of the edge in the x-direction of R_k in (33). We considered the symmetric sets

$$Q_k = \left(\frac{(k-1)\pi}{40}, \frac{k\,\pi}{40}\right) \times \left(-\frac{\pi}{150}, \frac{\pi}{150}\right) \bigcup \left(\frac{(40-k)\pi}{40}, \frac{(41-k)\pi}{40}\right) \times \left(-\frac{\pi}{150}, \frac{\pi}{150}\right). \tag{37}$$

In order to maintain the area constraint $|D| = \pi^2/225$, we sought the optimal position of 8 stiffened symmetric segments Q_k, but only close to the edges, that is,

$$\mathcal{D} = \text{the set of reunions of 4 symmetric segments } Q_k \text{ as in (37), for } k = 1, ..., 8\,. \tag{38}$$

We took again $\mathcal{F}$ as in (35) and we computed numerically the gap function for all the possible 70 configurations (the binomial of 8 and 4). We found that the optimal shape is $Q_2 \cup Q_4 \cup Q_6 \cup Q_8$, see the picture in Figure 12 where gray rectangles are the stiffened segments of deck. For this configuration we have $\mathcal{G}_D^\infty \approx 1.016 \cdot 10^{-3}$, $(\theta \approx 2.425 \cdot 10^{-2})$.

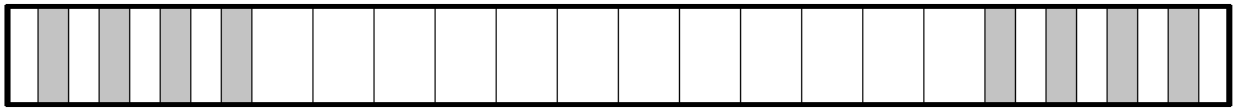

FIGURE 12. Solution of the minimaxmax problem (7) for $\mathcal{D}$ and $\mathcal{F}$ as in (38)-(35).

We refined further this procedure by taking smaller deck segments. We considered the symmetric sets

$$S_k = \left(\frac{(k-1)\pi}{80}, \frac{k\,\pi}{80}\right) \times \left(-\frac{\pi}{150}, \frac{\pi}{150}\right) \bigcup \left(\frac{(80-k)\pi}{80}, \frac{(81-k)\pi}{80}\right) \times \left(-\frac{\pi}{150}, \frac{\pi}{150}\right). \tag{39}$$

In order to maintain the area constraint $|D| = \pi^2/225$, we sought the optimal position of 16 stiffened symmetric segments S_k close to the edges, that is,

$$\mathcal{D} = \text{the set of reunions of 8 symmetric segments } S_k \text{ as in (39), for } k = 1, ..., 16\,. \tag{40}$$

We took again $\mathcal{F}$ as in (35) and we computed numerically the gap function for all the possible 12,870 configurations (the binomial of 16 and 8). We found that the optimal shape is $S_1 \cup S_3 \cup S_5 \cup S_7 \cup S_9 \cup S_{12} \cup S_{13} \cup S_{16}$ and, for this configuration, we have $\mathcal{G}_D^\infty \approx 1.011 \cdot 10^{-3}$, $(\theta \approx 2.413 \cdot 10^{-2})$.

Overall, these results enable us to conjecture that

$$\begin{gathered}\textbf{with no lower bound on the minimum size of the deck segments,}\\ \textbf{the optimal shape does not exist}\\ \textbf{and a minimizing sequence leads to homogenization}.\end{gathered} \tag{41}$$

Our results suggest that a minimizing sequence should be symmetric, having more stiff material close to the hinged edges.

5.2. **Optimal reinforcements with f defined by (25).** Next, we repeat the optimizations performed in the previous section, but now assuming that

$$\mathcal{F} = \{f\} \qquad \text{where } f \text{ is given by (25)} \tag{42}$$

since such f is conjectured (Conjecture 2) to be the optimal (worst) force for the free plate in the class $\{f \in L^\infty(\Omega);\ \|f\|_\infty = 1\}$.

Also in this case, the extremal values for the case of 4 stiffened rectangles R_k among the configurations in (34) were obtained for

$$D = R_1 \cup R_2 \cup R_{19} \cup R_{20} \implies \mathcal{G}_D^\infty \approx 2.7685 \cdot 10^{-4}\ (\theta \approx 6.609 \cdot 10^{-3})$$

$$D = R_9 \cup R_{10} \cup R_{11} \cup R_{12} \implies \mathcal{G}_D^\infty \approx 3.276 \cdot 10^{-4}\ (\theta \approx 7.821 \cdot 10^{-3})$$

and the principle (36) holds also when f is defined by (25).

Finally, we considered the optimization among configurations in (40) and the optimal solution was

$$D = S_1 \cup S_3 \cup S_5 \cup S_7 \cup S_9 \cup S_{11} \cup S_{13} \cup S_{15} \implies \mathcal{G}_D^\infty \approx 2.668 \cdot 10^{-4} \ (\theta \approx 6.369 \cdot 10^{-3}).$$

and this emphasized that the principle (41) should hold also in this case.

The classes $\mathcal{D}$ considered in the present section are all formed by a *finite number* of possible configurations and, therefore, problem (12) admits a solution. In fact, from Theorem 2 in [4] we know that the minimaxmax problem (12) admits an optimal shape D also if $\mathcal{D}$ consists of an infinite family of rectangles with inradius bounded away from 0 and free to move everywhere in Ω.

6. Optimal reinforcements made of small rectangles

In order to emphasize the possible appearance of homogenization [17], in this section we increase the number of rectangles and diminish their size, and we leave them free to move in Ω. We consider $\mathcal{D}$ defined by (19) for $P = 64$ and $\Delta x = \Delta y = \frac{\pi}{120}$, so that $\mathcal{D}$ contains 64 identical squares free to move in Ω. Note that with this choice of parameters we still have $|D| = \pi^2/225$, as in the previous section. Theorem 2 in [4] ensures again the existence of an optimal disposition of these squares reaching (12). However, the maximal gap varies very slowly while the squares move inside Ω and, numerically, it is quite difficult to find significant differences. In particular, our numerical procedure turned out to be very sensitive with respect to the initial choice of the initial vector $\mathcal{V}$.

The considered class $\mathcal{F}$ is again (35). We run the numerical algorithm for solving the optimization (12), starting from different initial vectors $\mathcal{V}$ randomly chosen. In Figure 13, we plot the optimal points (x_j, y_j), obtained in three numerical experiments. The algorithm was stationary for these configurations since, when we tried to restart the optimization procedure from those configurations, the cost functional did not decrease. The corresponding maximal gap is marked in each of the pictures.

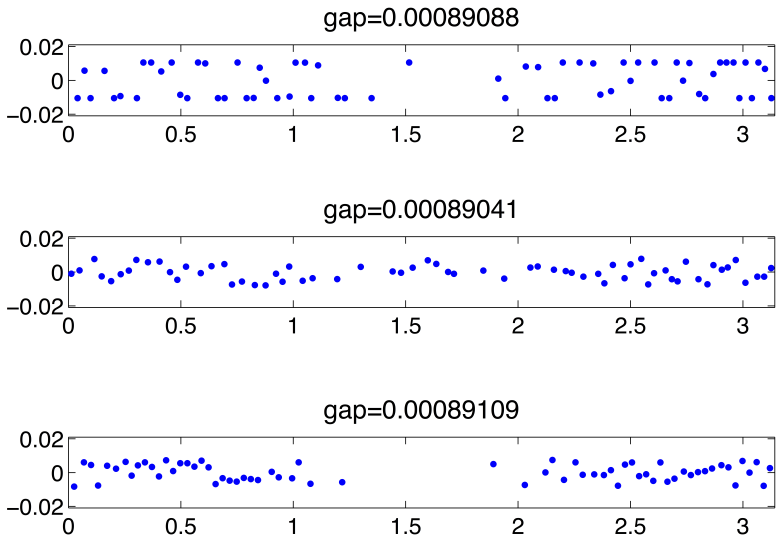

Figure 13. The points $(x_j, y_j), j = 1, ..., 64$ that we obtained in three numerical experiments.

In order to confirm the principle (36), we then started the optimization procedure with a vector $\mathcal{V}$ chosen in such a way that the initial squares were all concentrated close to the hinged edges, 32 of them close to each edge. The maximal gap obtained for this initial configuration was 9.5245×10^{-4}. In Figure 14, we plot the optimal points (x_j, y_j), obtained for this numerical experiment. The corresponding maximal gap, which was equal to 8.9071×10^{-4}, is marked in the picture and is approximately equal to those values obtained in the previous experiments.

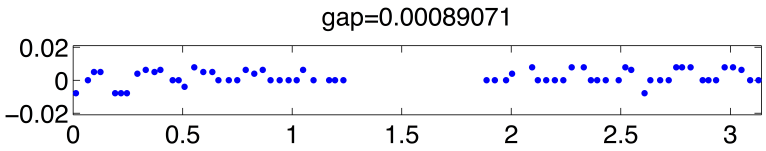

FIGURE 14. The points $(x_j, y_j), j = 1, ..., 64$ obtained in an experiment with a vector $\mathcal{V}$ chosen in such a way that the initial squares were all concentrated close to the hinged edges, 32 of them close to each edge.

The results in this section confirm the conjecture (41). Homogenization would lead to designs with reinforcements scattered throughout the structure, namely designs difficult to manufacture. At this point one has to make a choice. Either restrict the analysis to "macro" reinforcements (see e.g. [4, 19]) and ensure the existence of an optimal design D, or allow any kind of reinforcement at the price of losing existence of explicit and simple designs. In this paper we have mainly chosen small classes $\mathcal{D}$ of admissible geometries for D, but in future research it would be of some interest also to study the homogenization procedure.

7. Numerical results for a nonlinear problem

In this section we show some numerical results obtained for the minimaxmax problem related to the nonlinear equation (15). There are several suspension bridges in the world which are loaded by traffic in a fairly asymmetric way. This is the case of a bridge connecting a big city with some suburbs: in the morning the traffic flow goes towards the city, while in the evening it goes towards the suburbs. A typical example is the *Ponte 25 de Abril* in Lisbon [21]. Let us also recall the catastrophic failure of a bridge in Minneapolis, occurred during the evening rush hour on August 1, 2007, killing 13 people and injuring 145. According to the National Transportation Safety Boards investigation, roadway construction was underway on the deck-truss portion of the bridge, while four of its eight lanes were closed because of parked machineries and stock-piled paving materials on the bridge at the time of the collapse, see [12]. These facts show that it is of great interest also to consider *the static torsional equilibrium* of bridges crossed by cars.

In order to study the traffic loads in such cases, we view the plate Ω as a bridge with a roadway with four lanes, two for each direction of travel. We take π to measure 1km for the length of the main span. The bridge is crossed by cars which measure 4m×2m, that is, $\frac{\pi}{250} \times \frac{\pi}{500}$. Between two consecutive cars moving in the same direction, there is a security distance of at least 4m. Since there are 250 positions for the cars, this means that there are at most 125 cars in each lane. Between two parallel cars moving in the same direction but on different lanes there is a distance of $\frac{\pi}{1500} \approx$0.67m, while between the two directions of travel there is a separation barrier of width $\frac{\pi}{375} \approx$2.6m. All this is represented in Figure 15 where the two black regions are the components of ω in (13), the white lines are the separation of lanes whose amplitude is $\frac{\pi}{1500}$, the dark gray region is the separation barrier, the light gray rectangles are the possible positions of cars and they can be either empty or containing a car with the constraint that two consecutive rectangles in the direction of the traffic flow cannot both contain cars.

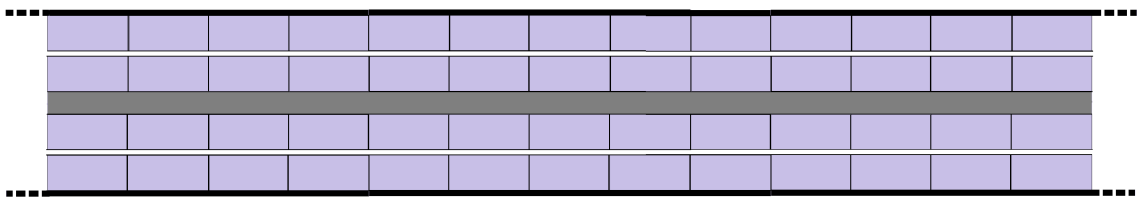

FIGURE 15. The roadway and the possible positions of the cars.

In order to identify the $250 \times 4 = 1,000$ rectangles (possible placements of the cars), we number the lanes from 1 to 4 starting from the upper lane in Figure 15 and we number the positions from 1 to 250 starting from the left in Figure 15. The rectangles T are then identified by two indices, $T = T_{i,j}$, with $i = 1, 2, 3, 4$ and $j = 1, ..., 250$.

Let us describe our results. In the first experiment we assumed that $D = \emptyset$ and we tested two cases that, in our opinion, are good candidates to be worst cases of the load. As for asymmetric (one-way) traffic flows, we considered 125 cars in each lane of same direction either "side to side" or in a "chessboard disposition", that is, we considered

$$\mathcal{F} = \{f_1, f_2\} \qquad \text{where} \qquad f_1 = \beta \sum_{j=1}^{125} \left(\chi_{1,2j-1} + \chi_{2,2j-1} \right), \qquad f_2 = \beta \sum_{j=1}^{125} \left(\chi_{1,2j-1} + \chi_{2,2j} \right). \tag{43}$$

Here, $\beta > 0$ denotes the density of mass of each car while $\chi_{i,j}$ denotes the characteristic function of the rectangle $T_{i,j}$. In Figure 16 we plot the maximal gap, as a function of the parameter β, just in the case of f_1: indeed, it turned out that the difference between $\mathcal{G}^{\infty}_{f_1}$ and $\mathcal{G}^{\infty}_{f_2}$ was very small, of order 10^{-13}.

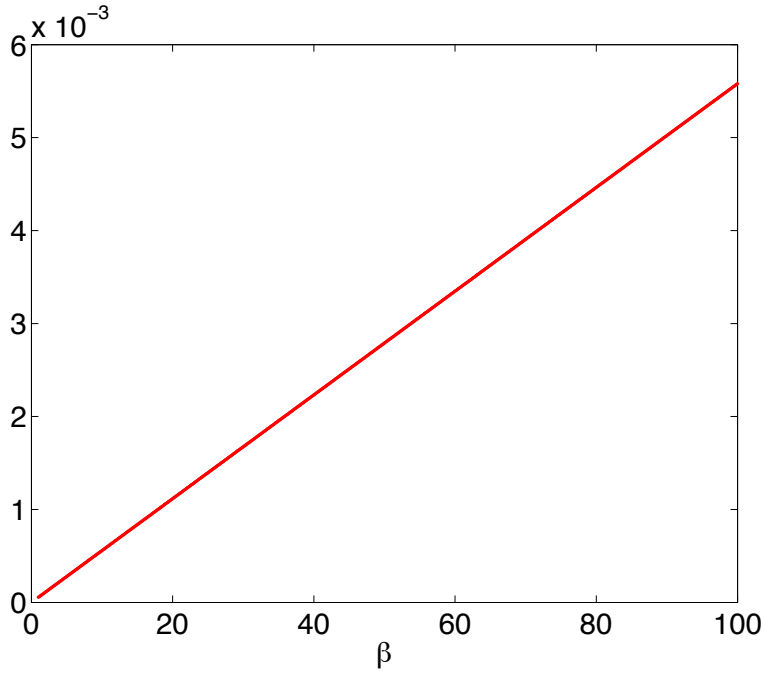

FIGURE 16. The maximal gap $\mathcal{G}^{\infty}_{f_1}$, as a function of the parameter β.

In the second experiment we restricted ourselves to $\mathcal{F} = \{f_1\}$, for four different choices of the mass β, and we sought the optimal position of 4 stiffened segments R_k among the 20 defined in (33), so that $\mathcal{D}$ was as in (34). In the three numerical experiments the optimal solution was always obtained for $D = R_1 \cup R_3 \cup R_{18} \cup R_{20}$, and the corresponding maximal gap was 4.5278282×10^{-5}, 4.5278258×10^{-4}, 4.5276550×10^{-3} and 4.5256308×10^{-2}, respectively for $\beta = 1, 10, 100, 1000$. Therefore, also for a simple nonlinear experiment, the principle (36) seems to hold.

8. Conclusions

Engineers are nowadays aware that many expensive optimization experiments in wind tunnels may be replaced by numerics, see e.g. the monograph [13], in particular its preface. From [13, p.13] we also also report the motivation of their work: *we are not trying to substitute a designer with these optimization techniques, which would be impossible because of the complexity of real problems, but rather intending to help a designer not to fall into false steps that can be very probable for a design with great complexity.*

This paper follows this motivation and tries to give hints on how to improve the torsional performance of rectangular plates modeling suspension bridges.

This target is pursued through the minimaxmax problem (7). After giving the correct variational formulation and explaining the numerical procedure sued throughout the paper, in Section 4 we studied the behavior of plates without a stiffening structure. We explained the differences between constraints on the loads in L^p spaces with large/small p, in particular for the *extremal and "physical" cases* $p = 1$ and $p = \infty$. The main results are summarized in Figures 3 and 7, leading to the conclusions (29) and (30).

Sections 5 and 6 consider stiffening structures made by rectangles, mainly motivated by the way of erecting bridges, see Figure 9. The main conclusions are (36) and (41). In particular, the possibility of having to deal with homogenization has to be taken seriously into account. This means that it could be preferable to consider stiffening structure made of mixture between materials rather than just of two distinct materials.

In Section 7 we made a first attempt to consider nonlinear problems, motivated by the nonlinear and nonlocal behavior of the sustaining cables. Even in this nonlinear setting, we reached the conclusion (36).

Acknowledgement. The Authors are grateful to the Editor and to two anonymous Referees for their suggestions and remarks that led to a substantial improvement of the present paper.

References

[1] G. Allaire, C. Dapogny, *A linearized approach to worst-case design in parametric and geometric shape optimization*, Math. Models Methods Appl. Sci. 24 no. 11, 2199-2257 (2014)

[2] G. Bartoli, P. Spinelli, *The stochastic differential calculus for the determination of structural response under wind*, J. Wind Engineering and Industrial Aerodynamics 48, 175-188 (1993)

[3] E. Berchio, D. Buoso, F. Gazzola, *A measure of the torsional performances of partially hinged rectangular plates*, In: Integral Methods in Science and Engineering, Vol.1, Theoretical Techniques, Eds: C. Constanda, M. Dalla Riva, P.D. Lamberti, P. Musolino, Birkäuser 2017, 35-46

[4] E. Berchio, D. Buoso, F. Gazzola, D. Zucco, *A minimaxmax problem for improving the torsional stability of rectangular plates*, J. Optim. Theory Appl. 177, 64-92 (2018)

[5] E. Berchio, A. Ferrero, F. Gazzola, *Structural instability of nonlinear plates modelling suspension bridges: mathematical answers to some long-standing questions*, Nonlin. Anal. Real World Appl. 28, 91-125 (2016)

[6] D. Braess, S. Sauter, C. Schwab, *On the justification of plate models*, J. Elasticity 103, 53-71 (2011)

[7] A. Cherkaev, E. Cherkaeva, *Principal compliance and robust optimal design*, J. Elasticity 72, 71-98 (2003)

[8] A. Ferrero, F. Gazzola, *A partially hinged rectangular plate as a model for suspension bridges*, Disc. Cont. Dynam. Syst. A 35, 5879-5908 (2015)

[9] F. Gazzola, *Mathematical models for suspension bridges*, MS&A Vol. 15, Springer (2015)

[10] H.-Ch. Grunau, *Nonlinear questions in clamped plate models*, Milan J. Math. 77, 171-204 (2009)

[11] H.-Ch. Grunau, G. Sweers, *A clamped plate with a uniform weight may change sign*, Discrete Contin. Dyn. Syst. Ser. S 7, 761-766 (2014)

[12] S. Hao, *I-35W Bridge collapse*, J. Bridge Eng. 15, 608-614 (2010)

[13] J.A. Jurado, S. Hernández, F. Nieto, A. Mosquera, *Bridge aeroelasticity, sensitivity analysis and optimal design*, WIT Press, Southampton (2011)

[14] B. Kawohl, J. Stará, G. Wittum, *Analysis and numerical studies of a problem of shape design*, Arch. Rat. Mech. Anal. 114, 349-363 (1991)

[15] C.F. Kollbrunner, K. Basler, *Torsion in Structures, An Engineering Approach*, Springer-Verlag Berlin Heidelberg (1969)

[16] J.L. Luco, J. Turmo, *Effect of hanger flexibility on dynamic response of suspension bridges*, J. Engineering Mechanics 136, 1444-1459 (2010)

[17] F. Murat, L. Tartar, *Calculus of variations and homogenization*, In: Topics in the Mathematical Modelling of Composite Materials, Vol. 31, Progr. Nonlin. Diff. Eq. Appl. 139-173 (1997)

[18] S.A. Nazarov, A. Stylianou, G. Sweers, *Hinged and supported plates with corners*, Zeit. Angew. Math. Physik 63, 929-960 (2012)

[19] S.A. Nazarov, G.H. Sweers, A.S. Slutskij, *Homogenization of a thin plate reinforced with periodic families of rigid rods*, Sbornik Mathematics 202, 1127-1168 (2011)

[20] W. Podolny, *Cable-suspended bridges*, In: Structural Steel Designers Handbook: AISC, AASHTO, AISI, ASTM, AREMA, and ASCE-07 Design Standards. By R.L. Brockenbrough and F.S. Merritt, 5^{th} Edition, McGraw-Hill, New York (2011)
[21] Ponte 25 de Abril, https://en.wikipedia.org/wiki/25_de_Abril_Bridge
[22] V. Torczon, *On the convergence of pattern search algorithms*, SIAM J. Optim., 7, 1-25 (1997).
[23] P. Villaggio, *Mathematical models for elastic structures*, Cambridge University Press, Cambridge (1997)
[24] E. Ventsel, T. Krauthammer, *Thin plates and shells: theory, analysis, and applications*, Marcel Dekker inc., New York (2001)
[25] S. Woinowsky-Krieger, *The effect of an axial force on the vibration of hinged bars*, J. Appl. Mech. 17, 35-36 (1950)

Pedro R.S. ANTUNES
Group of Mathematical Physics
Faculdade de Ciências da Universidade de Lisboa
Campo Grande, Edifício C6
1749-016 Lisboa, Portugal
prantunes@fc.ul.pt

Filippo GAZZOLA
Dipartimento di Matematica
Politecnico di Milano
Piazza Leonardo da Vinci 32, 20133
Milano, Italy
filippo.gazzola@polimi.it